Cellular/Molecular

Neuronal Differentiation in the Adult Hippocampus Recapitulates Embryonic Development

M. Soledad Espósito,* Verónica C. Piatti,* Diego A. Laplagne,* Nicolás A. Morgenstern, Carina C. Ferrari, Fernando J. Pitossi, and Alejandro F. Schinder

Fundación Instituto Leloir, 1405 Buenos Aires, Argentina

In the adult hippocampus and olfactory bulb, neural progenitor cells generate neurons that functionally integrate into the existing circuits. To understand how neuronal differentiation occurs in the adult hippocampus, we labeled dividing progenitor cells with a retrovirus expressing green fluorescent protein and studied the morphological and functional properties of their neuronal progeny over the following weeks. During the first week neurons had an irregular shape and immature spikes and were synaptically silent. Slow GABAergic synaptic inputs first appeared during the second week, when neurons exhibited spineless dendrites and migrated into the granule cell layer. In contrast, glutamatergic afferents were detected by the fourth week in neurons displaying mature excitability and morphology. Interestingly, fast GABAergic responses were the latest to appear. It is striking that neuronal maturation in the adult hippocampus follows a precise sequence of connectivity (silent → slow GABA → glutamate → fast GABA) that resembles hippocampal development. We conclude that, unlike what is observed in the olfactory bulb, the hippocampus maintains the same developmental rules for neuronal integration through adulthood.

Key words: **neurogenesis; dentate gyrus; plasticity; synaptogenesis; GABA; glutamate**

Introduction

The dentate gyrus (DG) of the mammalian hippocampus exhibits a peculiar development compared with the rest of the brain. The outer shell of the suprapyramidal blade of the granule cell layer (GCL) starts to be assembled during embryogenesis, but >80% of dentate granule cells (DGCs) are generated after birth (Angevine, 1965; Altman and Bayer, 1990). In rodents, the GCL is fully formed by postnatal day 30 (P30). At that time, neural progenitor cells (NPCs) become established at the subgranular zone (SGZ), where proliferation and neurogenesis continue for the entire life of the organism (Bayer et al., 1982; Altman and Bayer, 1990; Gage, 2000). A similar mechanism of cell renewal also occurs in the olfactory bulb (OB), where neuroblasts generated in the subventricular zone (SVZ) of the lateral ventricles migrate to the OB throughout adulthood (Lois and Alvarez-Buylla, 1994; Alvarez-Buylla et al., 2002).

Adult hippocampal neurogenesis has been observed in vertebrates from birds to humans (Nottebohm, 2002), yet its physiological significance remains essentially unknown (Schinder and Gage, 2004). However, increasing evidence points to a key role in hippocampal function. The basal rate of neurogenesis produces a significant amount of adult-generated neurons (Cameron and McKay, 2001). This rate is increased by enriched environment, voluntary exercise, specific learning paradigms, and pathological conditions such as seizures or ischemia (van Praag et al., 2000; Parent and Lowenstein, 2002; Kokaia and Lindvall, 2003). It is decreased by aging, stress, and depression (Duman, 2004). Moreover, manipulations affecting adult neurogenesis also alter hippocampus-dependent learning and behavior (Shors et al., 2001; Madsen et al., 2003; Santarelli et al., 2003). Finally, neurons derived from adult hippocampal NPCs make functional synapses *in vitro* (Toda et al., 2000; Song et al., 2002) and *in vivo* (van Praag et al., 2002; Liu et al., 2003; Schmidt-Hieber et al., 2004), supporting a functional role for hippocampal neurogenesis.

Proliferating NPCs exit the cell cycle to adopt one of the three neural phenotypes: astrocyte, oligodendrocyte, or neuron (Gage, 2000). To become a neuron, a cell must receive neurogenic cues to activate the appropriate genes to become excitable and synthesize and release neurotransmitters. In addition, it needs to migrate, mature, and establish presynaptic and postsynaptic connections. In the developing hippocampus, this process has been studied extensively (Lübbers and Frotscher, 1988; Laurie et al., 1992; Super and Soriano, 1994; Tyzio et al., 1999; Hennou et al., 2002; Gozlan and Ben Ari, 2003; Jones et al., 2003), but the sequence of events leading to neuronal maturation in the adult hippocampus remains unknown. Given the differences in the developing and adult environments, the process of maturation and the factors that modulate it may also differ. As an example, epileptic seizures increase adult neurogenesis (Parent et al., 1997)

Received July 27, 2005; revised Sept. 21, 2005; accepted Sept. 22, 2005.

This work was supported by the National Institutes of Health–Fogarty International Research Collaboration Award (RO3TW06130-01), Third World Academy of Sciences, the Fundación Antorchas, and Argentine National Agency for the Promotion of Science and Technology (ANPCyT) to A.F.S. A.F.S., C.C.F., and F.J.P. are investigators of the Argentine Research Council [Consejo Nacional de Investigaciones Científicas y Técnicas (CONICET)]. D.A.L. and M.S.E. were supported by CONICET. V.C.P. was supported by ANPCyT. We thank Henriette van Praag and Fred Gage for kindly providing the C11 retroviral packaging cell line and the NeuN antibody and Eric Olson and Christopher Walsh for the DCX antibody. We also thank Reiko M. Fitzsimonds, Fred Gage, Mary L. Gage, Juan Kamienkowski, and Hongjun Song for critical comments on this manuscript.

*M.S.E., V.C.P., and D.A.L. contributed equally to this work.

Correspondence should be addressed to Alejandro F. Schinder, Fundación Instituto Leloir, Patricias Argentinas 435, 1405 Buenos Aires, Argentina. E-mail: aschinder@leloir.org.ar.

DOI:10.1523/JNEUROSCI.3114-05.2005

 0270-6474/05/2510074-13$15.00/0

yet have opposite effects in the neonate DG (McCabe et al., 2001). Consistent with this notion, neurons generated in the adult SVZ arrive to the OB and receive synaptic inputs before they can spike, which is different from the sequence of events occurring during development (Carleton et al., 2003).

In the present work, we studied the morphological maturation and functional integration of neurons born in the adult DG and found a precise sequence that takes ~4 weeks and exhibits hallmarks that recapitulate hippocampal development.

Materials and Methods

Subjects and stereotaxic surgery. Female C57BL/6 mice, 6–7 weeks of age, were housed with a running wheel, which is known to enhance adult hippocampal neurogenesis, increasing the efficiency of viral transduction (van Praag et al., 1999). After 3 d, mice were anesthetized (100 μg ketamine/10 μg xylazine in 10 μl saline/g), and virus (1 μl at 0.15 μl/min) was infused into the right DG (anteroposterior, −2 mm from bregma; lateral, 1.5 mm; ventral, 1.9 mm) using a microcapillary calibrated pipette (Drummond Scientific, Broomall, PA).

Production of viral vectors. A retroviral vector based on the Moloney murine leukemia virus (MMLV) expressing enhanced green fluorescent protein (GFP) under a cytomegalovirus promoter was used (van Praag et al., 2002). The vector was produced by means of a stable NIT-GFP packaging cell line (clone 293gp/NIT-GFPc11; kindly provided by H. van Praag and F. H. Gage, Salk Institute, La Jolla, CA) that was transfected with pVSVG using Lipofectamine 2000 (Invitrogen, San Diego, CA). Virus-containing supernatant was harvested 48 h after transfection and concentrated by two rounds of ultracentrifugation.

Electrophysiology. Experiments were performed in slices from 102 mice. Mice were anesthetized and decapitated between 1 and 29 d after surgery. Brains were removed into a chilled solution containing the following (in mM): 110 choline-Cl^-, 2.5 KCl, 2.0 NaH_2PO_4, 25.0 $NaHCO_3$, 0.5 $CaCl_2$, 7 $MgCl_2$, 20 dextrose, 1.3 Na^+-ascorbate, 0.6 Na^+-pyruvate, and 4.0 kynurenic acid (kyn). Horizontal slices, 300 μm thick, were cut in a vibratome and transferred to a chamber containing the following (in mM): 125.0 NaCl, 2.5 KCl, 2.0 NaH_2PO_4, 25.0 $NaHCO_3$, 2 $CaCl_2$, 1.3 $MgCl_2$, 1.3 Na^+-ascorbate, 3.1 Na^+-pyruvate, and 10 dextrose (315 mOsm). The slices were bubbled with 95% O_2/5% CO_2 and maintained at 30°C. Recordings were performed at 23 ± 2°C using microelectrodes (5–8 MΩ) pulled from borosilicate glass (KG-33; Garner Glass, Claremont, CA) and filled with the following (in mM): 120.0 K-gluconate, 20 KCl, 5 NaCl, 4 $MgCl_2$, 0.1 EGTA, 10.0 HEPES, 4.0 Tris-ATP, 0.3 Tris-GTP, 10 phosphocreatine, Alexa Fluor 594 (5 μg/ml; Invitrogen), pH 7.3, and 290 mOsm. A junction potential of 11 mV was calculated according to Barry and Lynch (1991). For the experiments performed with symmetrical Cl^- (supplemental Fig. S2*D*, available at www.jneurosci.org as supplemental material), K-gluconate and KCl were replaced by 140 mM CsCl. Unless otherwise noted, all chemicals were obtained from Sigma (St. Louis, MO).

GFP^+ cells were identified in the granule cell layer using FITC fluorescence optics (DMLFS; Leica, Nussloch, Germany). GFP^- DGCs localized near the GFP^+ cells were used as controls in paired experiments. Sections surrounding the injection site displaying signs of inflammation were discarded. Whole-cell recordings (Axopatch 200B; Molecular Devices, Union City, CA) were filtered at 2 kHz, digitized (Digidata 1322A; Molecular Devices), and acquired onto a personal computer using jClamp (SciSoft, New Haven, CT). Series resistance was typically 10–40 MΩ. Voltage-clamp experiments were performed at a holding potential (V_{Hold}) of −80 mV, unless otherwise noted. Criteria to include cells in the analysis were colabeling with Alexa Fluor 594 or visual confirmation of GFP in the pipette tip and absolute leak current <100 pA at V_{Hold}. Membrane capacitance and input resistance were measured in response to a hyperpolarizing voltage step of 10 mV. Passive membrane properties were monitored also at 42–49 d postinfection (dpi) mice. In current-clamp recordings, the resting membrane potential was kept at −80 mV by passing a constant holding current. The presence of action potentials in GFP^+ cells was assessed by depolarizing current steps (10 pA; 50 or 500 ms) until a maximum membrane potential of 0 mV. Spike amplitude was measured between the beginning of the fast rising phase and the first peak. The afterhyperpolarization (AHP) amplitude was assessed with respect to the steady-state value after recovery.

Extracellular stimulation (0.1 Hz) was done using concentric bipolar electrodes (50 μm diameter; Frederick Haer Company, Bowdoinham, ME), a Grass S88 stimulator, and a stimulus isolation unit (SIU5; Grass Instruments, Quincy, MA). The stimulation electrode was placed on the GCL ~250 μm away from the recorded cell. Functional inputs were assessed at a stimulus strength of 15–20 V (50 μs), and a neuron was considered to be silent when it did not respond to 30 V, but one adjacent control DGC did. Amplitude, rise (20–80%), and decay times (peak to 40%) were measured off-line using software routines written by D. A. Laplagne.

For cells with one GABA component, G_{max} was measured as the slope of the *I–V* curve, and the reversal potential (E_{GABA}) was calculated from the linear fit. When two components were present, the reversal potentials were interpolated from the corresponding *I–V* curves measured at the time of the peak (for the early fast component) and 85 ms after the onset of the stimulus (for the late slow component). Fast and slow conductances were calculated as the ratio between the peak current amplitude at the reversal potential of the opposite component and the corresponding driving force. All example traces of evoked responses are averages of more than five sweeps.

Spontaneous activity was filtered at 2 kHz and rise time (10–90%), decay time (peak to 40%), and amplitude were measured off-line using Mini Analysis software (Synaptosoft, Decatur, GA). Recordings of spontaneous activity lasted >10–15 min, and a cell was considered to be synaptically active when >1 event per minute was found. The presence of extrasynaptic receptors was assessed by focal application of agonists near the soma using a homemade perfusion system.

For somatic blockade of GABAergic currents, 1 mM bicuculline methiodide (BMI) was pressure ejected from a glass pipette ~10–20 μm away from the soma and pointing toward the hilus in pulses of 10–20 ms at 1–4 Hz with a pressure of <2 psi (Pressure System IIe; Toohey Company, Fairfield, NJ). Alexa Fluor 594 (5 μg/ml) was added to monitor and control the spread of the local perfusion.

Immunocytochemistry and confocal microscopy. Immunostaining was done on 40 μm free-floating coronal sections throughout the hippocampus, analyzing up to one every three sections to obtain >50 GFP^+ cells/mouse. Antibodies were applied in TBS with 3% donkey serum and 0.25% Triton X-100. Neuronal-specific nuclear protein (NeuN; mouse monoclonal; 1:50; a gift from F. H. Gage), doublecortin (DCX; rabbit polyclonal; 1:750; a gift from C. Walsh, Harvard Medical School, Cambridge, MA), and GFP (chicken polyclonal; 1:500; Invitrogen) antibodies were combined. Corresponding secondary antibodies were used [donkey anti-mouse cyanine 5 (Cy5), donkey anti-rabbit Cy3, donkey anti-chicken Cy2; 1:250; Jackson ImmunoResearch, West Grove, PA]. Sections surrounding the injection site displaying signs of inflammation were discarded. All analyses were performed in triple-stained sections (GFP, DCX, and NeuN) using a Zeiss Pascal confocal microscope (Zeiss, Thornwood, NY). Only GFP^+ cells located in the SGZ or GCL were included in the analysis. Expression of markers and localization were done counting >50 GFP^+ cells per mouse. Colocalization was assessed through the entire *z*-axis of each cell, using an optical slice of 0.7–1 μm. Morphology was analyzed from three-dimensional reconstructions of a series of confocal images taken at 0.7–1 μm intervals in GFP^+ neurons from more than three mice each.

Results

The purpose of this study was to characterize the differentiation and maturation of DGCs generated in the adult hippocampus. To achieve this goal, proliferating NPCs were labeled by injecting a retroviral construct that expresses GFP in the DG of C57BL/6J adult female mice (6–7 weeks of age). The morphology and distribution of GFP-positive (GFP^+) neurons were monitored by immunofluorescence and confocal microscopy in fixed brain sections (40 μm thick) at 7, 14, and 28 dpi. In these experiments, neuronal phenotype was determined by the expression of specific

neuronal markers. Neuronal function was studied by whole-cell patch-clamp recordings performed in GFP$^+$ cells from acute brain slices (300 μm thick) collected from 1 to 29 dpi. Recorded neurons were identified on the basis of their ability to spike in response to depolarizing steps in current-clamp recordings. Both approaches converged in the existence of distinctive stages of neuronal maturation that are described below.

Morphology and distribution of 7-d-old neurons

The degree of neuronal maturity was determined by the expression of early and late neuronal markers and the analysis of cell morphology. DCX, a microtubule-associated protein expressed during neuronal migration, was used as a marker for immature neurons (Gleeson et al., 1999; Tanaka et al., 2004). NeuN, a neuronal nuclear antigen, was used as a constitutive neuronal marker (Mullen et al., 1992). In the adult DG, DCX was expressed in the soma and dendrites of neurons located in the inner layers of the GCL, near the SGZ (Fig. 1*B*). In general, the dendritic arborization of neurons expressing DCX reached, at most, the middle molecular layer. NeuN labeled the nucleus of DGCs throughout the GCL (Fig. 1*A*) (van Praag et al., 2002; Kempermann et al., 2003; Garcia et al., 2004). Expression of neuronal markers in the progeny of NPCs was assessed by colocalization of GFP with DCX (Cy3 label) and/or NeuN (Cy5 label) in multiple confocal planes through the *z*-axis of the entire soma and proximal processes (see Materials and Methods). Thus, GFP$^+$ cells expressing DCX and/or NeuN were defined as neurons.

From a total of 310 GFP$^+$ cells analyzed from five mice at 7 dpi, 46 expressed only DCX, 95 showed simultaneous expression of DCX and NeuN, and 13 expressed NeuN alone (Fig. 1*D*,*E*,*H*), resulting in ~50% of GFP$^+$ cells exhibiting a neuronal phenotype. The fluorescence intensity of NeuN in immature neurons was somewhat lower than that of mature neurons. Complete three-dimensional reconstructions of cells at this stage ($n = 64$) evidenced immature morphological features that could be fitted into two categories that we defined as class A and class B neurons. Class A neurons showed a large irregular soma with or without processes of short length and variable thickness, running parallel to the GCL (Fig. 1*F*) ($n = 28$). Class B neurons exhibited an oval-shaped soma with longer processes, also parallel to the GCL or turning toward the GCL (Fig. 1*G*) ($n = 36$). Neurons with more mature granule cell morphology were not observed at this time, not even in the minor population that expressed exclusively NeuN. Although NeuN has been commonly used as a marker for mature neurons, our observations underscore an early onset of NeuN expression in neuronal differentiation.

Because adult-born DGCs migrate radially from the SGZ deeper into the GCL (Altman and Bayer, 1990; Kempermann et al., 2003), migration of GFP$^+$ neurons was assessed by their relative position in the GCL. To obtain a quantitative score of the position, the GCL was divided from inner to outer layers in GCL 1, GCL 2, and GCL 3, and each cell was assigned to one of these layers or the SGZ (Fig. 1*C*). At 7 dpi, newly generated neurons were observed isolated or in clusters, and their distribution seemed to be independent of the neuronal markers, because most cells were located at the SGZ, and only a small fraction was positioned in GCL 1 (Fig. 1*A*,*B*,*H*).

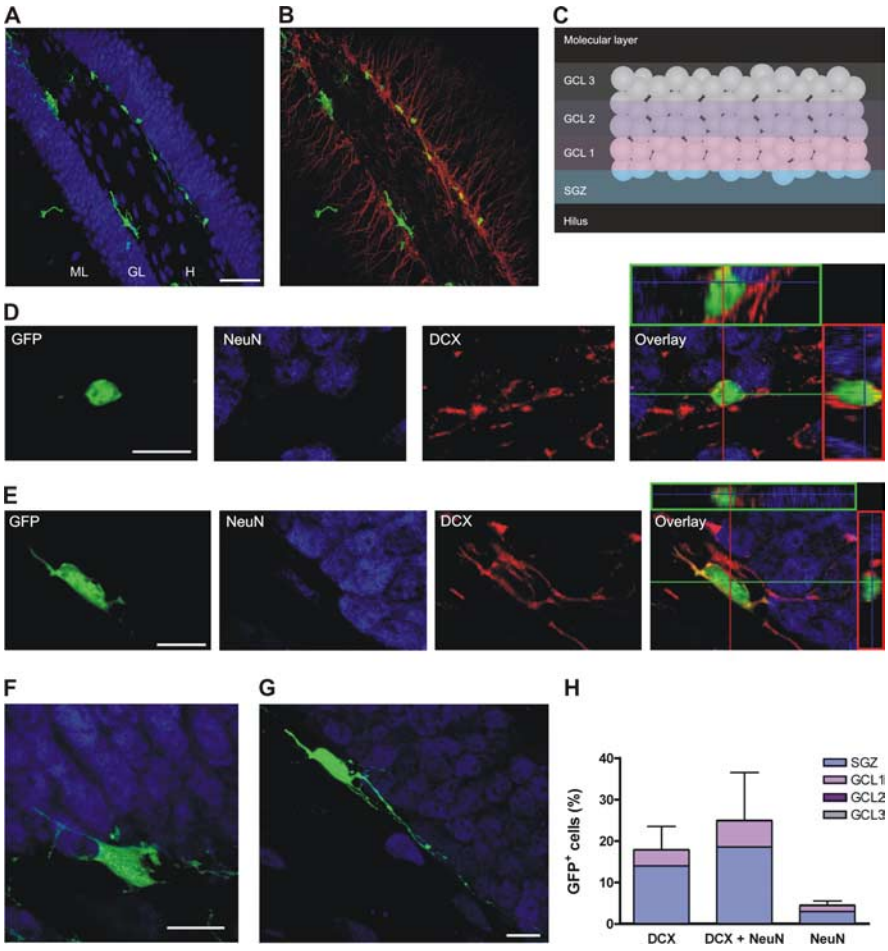

Figure 1. Morphology of class A and B neurons at 7 dpi. ***A***, ***B***, Overview of a transverse section of the DG showing the subgranular localization of GFP$^+$ cells (green). NeuN is shown in blue (***A***), and DCX is shown in red (***B***). Images are merges of 33 confocal planes. Scale bar, 50 μm. ML, Molecular layer; GL, granule cell layer; H, hilus. ***C***, Schematic diagram depicting the subdivisions of the GCL. ***D***, ***E***, Examples of a GFP$^+$ cell colocalizing with DCX alone (***D***) and a cell expressing DCX and NeuN (***E***). A single optical section is shown to the left for the green, blue, and red channels. Their overlay is shown in the right panel, together with the orthogonal projections onto the *x*–*z* (top) and *y*–*z* (right) planes. ***F***, ***G***, Typical examples of class A (***F***) and class B (***G***) neurons. Confocal images are projections of 30 optical slices onto the *x*–*y* plane. ***H***, Distribution of GFP$^+$ cells expressing neuronal markers, normalized to the total number of GFP$^+$ cells. Each bar was calculated as the mean percentage of cells expressing the corresponding marker and its SEM ($n = 5$ mice). Internal subdivisions are also included to indicate the distribution within the GCL. No significant differences were observed in the percentage of expression of the different markers ($p = 0.17$; ANOVA). Scale bars: ***D–G***, 10 μm.

Physiology of developing neurons

GFP$^+$ cells were identified as neurons ($n = 164$) by their capacity to generate action potentials. Interestingly, spiking cells were detected as early as 1 dpi (Fig. 2*A*). The following passive membrane properties were monitored: input resistance (R_{input}), which is a function of both the area of the cell membrane and the ion channel density; membrane capacitance (C_m), which is proportional to the area of the soma and proximal dendrites; and resting po-

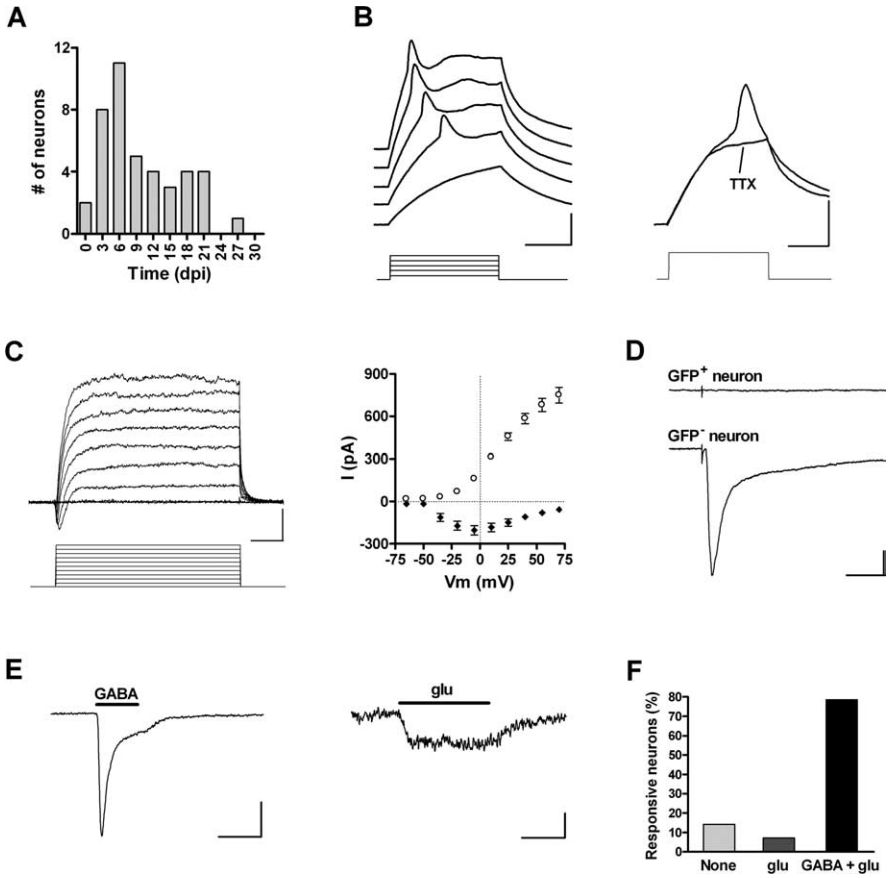

Figure 2. Electrophysiology of silent neurons. ***A***, Age of GFP $^+$ neurons exhibiting action potentials and lacking synaptic inputs ($n = 42$). ***B***, Left, Depolarizing current steps (10 pA) elicit short and wide action potentials in a 5 dpi neuron. Right, Immature spikes are blocked by 1 μM TTX (step, 20 pA). Calibration: 20 mV, 20 ms. ***C***, Left, Depolarizing voltage steps (15 mV) elicit fast inward and slow outward currents in a 4 dpi neuron. Calibration: 200 pA, 5 ms. Right, *I–V* plot of peak inward current (filled diamonds) and steady-state outward current (open circles). Data are mean ± SEM ($n = 35$). ***D***, Lack of postsynaptic responsiveness of a GFP $^+$ neuron (top trace) to extracellular stimulation of the GCL (30 V, 50 μs). A neighboring GFP $^-$ neuron did exhibit a complex inward current in response to the same stimulus (bottom trace). Calibration: 50 pA, 30 ms. ***E***, Responses of a 4 dpi neuron to focal application of 0.5 mM GABA (I_{peak}, −98.6 ± 24.5 pA; $n = 11$; left) and 0.5 mM glu (I_{peak}, −12.1 ± 2.5 pA; $n = 11$; right). Calibration: 50 pA (left), 5 pA (right), 10 s. ***F***, Percentage of GFP $^+$ neurons responding to exogenous application of GABA and glu ($n = 14$ cells).

tential (V_{rest}), which is determined by the relative ionic concentrations and permeabilities (supplemental Fig. S1*A–C*, available at www.jneurosci.org as supplemental material). During the early stages of maturation, neurons displayed a high R_{input} and low C_m, properties that are typical of immature neurons in the developing and adult brain (Owens et al., 1996; Carleton et al., 2003; Zhang, 2004; Overstreet Wadiche et al., 2005; Ye et al., 2005). Over time, R_{input} decreased and C_m increased to reach levels that are characteristic of mature DGCs. A depolarized V_{rest} was found in immature DGCs compared with the control GFP $^-$ neurons, but this is most likely a result of the technical difficulties associated with measuring membrane potential in neurons with a high input resistance (Tyzio et al., 2003). In contrast, nonspiking cells ($n = 92$) exhibited a low R_{in} (median, 105 MΩ; range, 12–9100 MΩ) and C_m (median, 8.8 pF; range, 2.1–73.5 pF) and a more hyperpolarized V_{rest} (median, −71 mV; range, −30 to −89 mV) than spiking neurons at immature ages. This population might include nondifferentiated progenitors, astrocytes, oligodendrocytes, and/or very immature neurons and, consequently, no additional analysis was performed on these cells.

An incipient excitability in immature neurons was revealed by the small amplitude of action potentials and inward Na^+ and outward K^+ currents. These amplitudes increased over time and reached values similar to those of mature neurons after ~4 weeks (supplemental Fig. S1*D–F*, available at www.jneurosci.org as supplemental material). Despite the fact that passive and active membrane properties seemed to develop gradually, discrete stages of neuronal maturation became apparent as afferent connectivity was examined.

Afferent connectivity was assessed by the presence or absence of evoked synaptic responses, and their GABAergic or glutamatergic nature was pharmacologically determined. This analysis, which was performed in 90 neurons of all ages (1–29 dpi), revealed the existence of three functional groups: (1) neurons without input or "silent" ($n = 42$; median, 7 dpi); (2) neurons with only GABAergic inputs ($n = 24$; median, 18 dpi), and (3) neurons bearing both GABAergic and glutamatergic afferent connections ($n = 24$; median, 26 dpi). Neurons belonging to each of these discrete groups were pooled and are described in detail below.

Early immature neurons lack afferent inputs

A GFP $^+$ neuron was considered to be silent when extracellular stimulation of the GCL failed to induce postsynaptic responses even at high stimulus strengths while eliciting postsynaptic currents (PSCs) in adjacent nonlabeled neurons (Fig. 2*D*) ($n = 42$). Neurons without evoked PSCs also failed to exhibit spontaneous synaptic activity ($n = 7$). All GFP $^+$ neurons studied between 1 and 7 dpi were silent, and their morphology (as seen under fluorescence microscopy) seemed to correspond to class A or B. At later time points, as GABAergic afferents became connected (see below), the number of silent neurons decreased. However, a few neurons of this sort were still observed as late as 21 dpi (Fig. 2*A*). Silent neurons displayed high R_{input} and low C_m (Table 1). Depolarizing current steps elicited a single spike of small amplitude and long duration that was blocked by 1 μM tetrodotoxin (TTX) (blockade, 101.0 ± 3.5%; $n = 7$) (Fig. 2*B*). In agreement with this incipient excitability, voltage-clamp recordings rendered weak inward Na^+ currents and larger outward K^+ currents in 36 of 40 spiking cells (Fig. 2*C*, Table 1). The remaining neurons failed to show detectable Na^+ currents, presumably because of a low signal-to-noise ratio. Nevertheless, immature neurons with a high R_{input} would require very small inward currents to spike.

The lack of synaptic responses in early immature neurons might be a result of the absence of functional synaptic terminals or to the lack of appropriate neurotransmitter receptors. To address this issue, neurons were challenged with focal application of GABA (0.5 mM) and glutamate (glu) (0.5 mM), and responses

were recorded under voltage or current clamp (Fig. 2*E*,*F*). Most cells responded to both agonists, indicating that neurotransmitter receptors are already present in the plasma membrane before the arrival of presynaptic terminals. Together, these results demonstrate that the expression of neurotransmitter receptors and the onset of excitability are primary features of early neuronal differentiation and occur before the arrival of afferent connections. The early appearance of glu and GABA receptors has also been described in embryonic cortical progenitor cells (LoTurco et al., 1995), developing CA1 pyramidal neurons (Tyzio et al., 1999), and neuroblasts from the adult SVZ (Carleton et al., 2003).

Morphology and distribution of 14-d-old neurons

Immunofluorescence analysis at 14 dpi showed qualitative differences in neuronal phenotype and distribution compared with 7dpi (Fig. 3*A*). Although no change was observed in the percentage of GFP$^+$ cells expressing neuronal markers (~50%), there was a significant increase in the coexpression of DCX and NeuN, which was accompanied by a more differentiated neuronal morphology (Fig. 3*B*,*C*). The most prominent feature of the predominant morphology (named class C; $n = 60$) was an apical dendritic tree with no spines extending through the GCL and reaching the middle molecular layer (maximal distance from soma, 81 ± 7 μm; $n = 5$) (Fig. 3*D*,*E*). In most cases, we also observed basal dendrites projecting to the hilus that retract at later stages of maturation. These cells exhibited a total dendritic length of 185 ± 13 μm and 6.0 ± 1.3 branching points ($n = 5$). Neurons at this stage had already migrated into the GCL and were concentrated primarily within GCL1, with ~20% of the cells reaching GCL2 (Fig. 3*B*). These results indicate that neurons at 14 dpi have developed further, but they are still immature compared with fully differentiated DGCs (van Praag et al., 2002). In addition, the lack of dendritic spines in class C neurons indicates that functional glutamatergic inputs have not yet been established, which was further confirmed by electrophysiological recordings.

The onset of GABAergic connectivity

The morphological maturation described above was paralleled by an increased excitability and by the presence of GABAergic afferents (Fig. 4). Neurons with GABAergic but not glutamatergic afferents were first observed at 8 dpi and displayed lower

Table 1. Membrane properties of neurons at discrete stages of maturation

	Silent	GABA	GABA and glu	GFP$^-$ neurons
V_{rest} (mV)	−50.6 ± 2.3 (37)	−45.6 ± 2.3 (24)*	−63.2 ± 2.8 (24)***	−74.3 ± 0.7 (118)
C_m (pF)	6.4 ± 0.4 (42)	11.7 ± 1.2 (24)*	24.6 ± 1.4 (24)***	38.8 ± 1.2 (126)
R_{input} (GΩ)	4.3 ± 0.5 (42)	2.9 ± 0.4 (24)**	0.62 ± 0.10 (24)**	0.31 ± 0.14 (126)
G_m/C_m (pS/pF)[a]	65 ± 8 (42)	54 ± 8 (24)**	110 ± 19 (24)	111 ± 6 (126)
AP peak (mV)[b]	17.0 ± 1.7 (41)	43.8 ± 3.7 (23)**	83.5 ± 3.1 (24)	92.9 ± 1.2 (98)
Peak I_{in} (nA)[c]	−0.17 ± 0.03 (36)	−1.04 ± 0.30 (24)***	−4.2 ± 0.5 (23)	−5.4 ± 0.3 (98)
Maximum I_{out} (nA)[d]	0.72 ± 0.05 (39)*	1.5 ± 0.2 (24)**	3.4 ± 0.3 (23)	3.8 ± 0.2 (98)

Data from GFP$^+$ neurons were grouped by afferent connectivity and correspond to those in Figure 2 (silent), Figure 4 (GABA), and Figures 6–8 (GABA and glu). The GFP$^-$ neuron group summarizes values obtained from unlabeled neurons recorded between 1 and 29 dpi. Values are mean ± SEM. The number of cells tested is indicated in parentheses. Differences between groups were analyzed using a Kruskal–Wallis test followed by a *post hoc* Dunn's test to compare each group with its neighbor on the right. *$p < 0.05$; **$p < 0.01$; ***$p < 0.001$. AP, Action potential; G_m, membrane conductance.

[a]Provides a measure of the density of the leak conductance.

[b]Measured in the first action potential of the spike train.

[c]Inward current measured at $V_{hold} = -20$ mV.

[d]Outward current measured at steady state ($V_{hold} = +70$ mV).

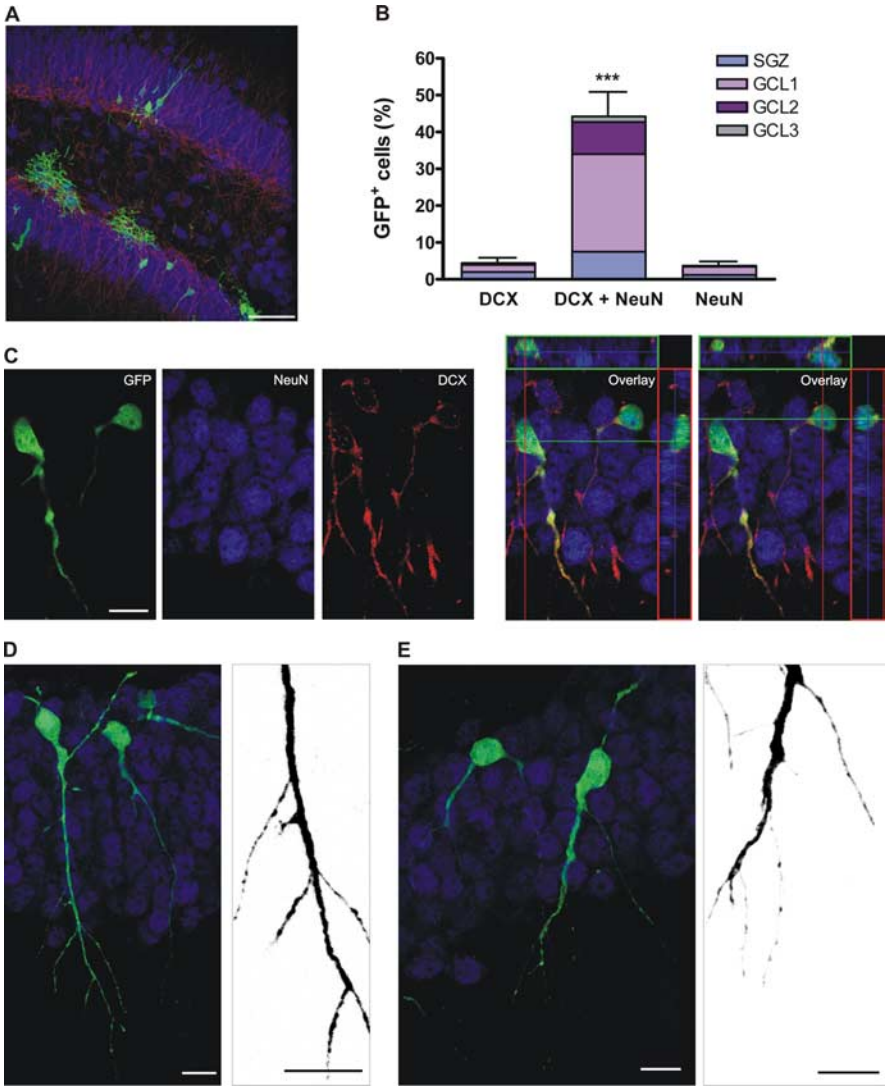

Figure 3. Morphological features of class C neurons at 14 dpi. ***A***, Transverse section of the DG showing the localization of GFP$^+$ cells. The image is a merge of 27 confocal planes. Scale bar, 50 μm. ***B***, Distribution of GFP$^+$ cells expressing neuronal markers, normalized to the total number of GFP$^+$ cells. Bars show mean ± SEM percentage of cells expressing the corresponding marker ($n = 399$ GFP$^+$ cells from 6 mice). ***$p < 0.001$ by ANOVA with *post hoc* Bonferroni's test. ***C***, Example of two adjacent neurons expressing DCX and NeuN in the same optical section and the overlays together with their corresponding orthogonal projections. ***D***, ***E***, Examples of class C neurons. Images are projections of 23 (***D***) and 12 (***E***) optical sections. Micrographs taken with a higher digital zoom (right panels) depict details of spineless dendrites (merge of 11 and 5 confocal planes taken at 0.7 μm intervals, respectively). Cells shown in ***E*** are the same as in ***C*** but rotated 180° for clarity. Scale bars: ***C–E***, 10 μm.

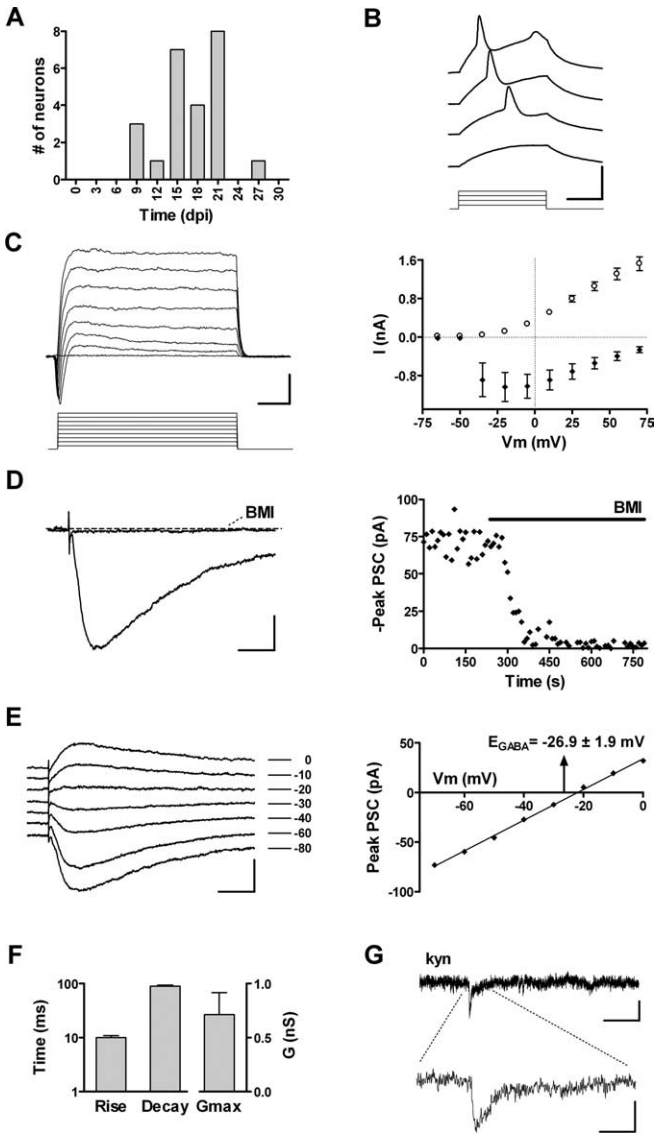

Figure 4. Functional properties of neurons with GABAergic inputs. ***A***, Age of GFP$^+$ neurons exhibiting only GABAergic afferents ($n = 24$). ***B***, Depolarizing current steps (10 pA) elicit immature action potentials in a 20 dpi neuron. Calibration: 50 mV, 20 ms. ***C***, Left, Depolarizing voltage steps (15 mV) evoke fast inward and slow outward currents in a 19 dpi neuron. Calibration: 400 pA, 5 ms. Right, *I–V* plot of peak inward current (filled diamonds) and steady-state outward current (open circles). Data are mean ± SEM ($n = 24$). ***D***, Left, GABAergic postsynaptic currents of a 22 dpi neuron in response to extracellular stimulation of the GCL (20 V, 0.1 Hz) are fully blocked by 20 μM BMI. Calibration: 20 pA, 25 ms. Right, Peak $GABA_A$-mediated current before and during BMI application measured from the cell shown on the left. The horizontal bar depicts the duration of antagonist perfusion. ***E***, Left, Example of evoked GABAergic PSCs recorded at V_{Hold} shown to the right from a 22 dpi neuron. Calibration: 40 pA, 25 ms. Right, *I–V* curve of the peak GABAergic PSCs shown to the left. The arrow denotes mean ± SEM of E_{GABA} ($n = 10$ cells). ***F***, Rise time, decay time ($n = 24$), and conductance (G_{max}; $n = 10$) of evoked GABAergic PSCs. Bars represent mean ± SEM. ***G***, Spontaneous GABAergic PSCs recorded from a 25 dpi neuron are insensitive to kyn (4 mM). Calibration: 4 pA, 400 ms (top trace), 40 ms (bottom trace).

R_{input} and higher C_m than silent neurons (Fig. 4*A*, Table 1). Spike amplitude increased, as did the voltage-gated inward Na^+ and outward K^+ currents (Fig. 4*B*,*C*). In addition, a small afterhyperpolarization became apparent (AHP_{peak}, −6.1 ± 1.1 mV; $n = 8$). However, depolarizing current steps still elicited one or few spikes but not the repetitive spiking typical of mature DGCs. Interestingly, extracellular stimulation of the GCL evoked slow inward currents that were insensitive to kyn (4 mM), an antagonist of ionotropic glu receptors (blockade, 3.4 ± 3.1%; $n = 11$) but were fully blocked by BMI (20 μM), a specific antagonist of $GABA_A$ receptors (94.6 ± 1.3%; $n = 10$) (Fig. 4*D*). The kinetics of these $GABA_A$-mediated PSCs is reminiscent of slow dendritic responses rather than fast perisomatic currents described in hippocampal neurons (Fig. 4*F*) (Pearce, 1993; Soltesz et al., 1995; Banks et al., 1998). In adjacent nonlabeled neurons, extracellular stimulation of the same pathway evoked mixed GABAergic and glutamatergic PSC (data not shown). In agreement with the high permeability of $GABA_A$ receptors to Cl^- (Kaila, 1994), GABAergic-evoked PSCs displayed a reversal potential (E_{GABA}) of −26.9 ± 1.9 mV (Fig. 4*E*), which, after correction for an electrode junction potential of 11 mV, is close to the Cl^- equilibrium potential (E_{Cl^-}) of −36 mV predicted for our whole-cell recording conditions.

Spontaneous synaptic activity was insensitive to kyn (Fig. 4*G*), but it was fully blocked by BMI (data not shown), which further supports the GABAergic nature of functional synaptic inputs onto immature neurons. Spontaneous PSCs displayed a low frequency (0.05 ± 0.02 Hz; $n = 6$) and long rise and decay times (rise, 12.1 ± 2.5 ms; decay, 34.0 ± 6.8 ms) (supplemental Fig. S2*A*, available at www.jneurosci.org as supplemental material), consistent with the slow kinetics exhibited by evoked PSCs. The slow kinetics of GABAergic PSCs suggests a dendritic localization of the early GABAergic connections (see Discussion) (Miles et al., 1996; Banks et al., 1998, 2002). These findings demonstrate that GABAergic interneurons are the primary source of synaptic inputs onto immature neurons in the adult hippocampus, similar to what occurs to CA1 pyramidal neurons and DGCs during development (Tyzio et al., 1999; Khazipov et al., 2001; Gozlan and Ben Ari, 2003).

Morphology and distribution of 28-d-old neurons: the final steps of neuronal maturation

The proportion of GFP$^+$ cells expressing neuronal markers at 28 dpi was similar to the previous developmental stages (see Fig. 9*A*) but still lower than in previous reports using bromodeoxyuridine (BrdU) to label neuronal proliferation. This is likely caused by differences in the mechanisms of action between retroviral labeling and BrdU. In fact, transgene downregulation has been demonstrated for MMLV retrovirus, and it depends on the degree of differentiation and on the site of viral integration into the genome of the host cell (Xu et al., 1989). Indeed, we observed that mature neuronal cells exhibited a lower intensity of GFP fluorescence when compared with immature neurons or other GFP$^+$ cell types, similar to previous studies using the same retroviral construct (van Praag et al., 2002). Therefore, the percentage of adult-born neurons with a mature phenotype may be underestimated in our experimental conditions.

GFP$^+$ neurons at 28 dpi showed mature features, consistent with previous observations (van Praag et al., 2002). The vast majority of cells expressed NeuN exclusively and was still localized in GCL 1 (Fig. 5*A–C*). These neurons (class D; $n = 34$) displayed a round soma, a conspicuous axonal projection extending toward the hilus, and spiny dendrites reaching the outer molecular layer (Fig. 5*D*,*E*). Although the number of branching points (7.0 ± 0.5; $n = 5$) was similar to that of class C neurons ($p = 0.84$; Mann–Whitney test), the total dendritic length (627 ± 82 μm), and the maximal distance from the soma (186 ± 15 μm) were significantly larger ($n = 5$; $p < 0.001$; *t* test for both). Dendritic spines were prominent throughout the molecular layer, suggesting the presence of glutamatergic synapses. Interestingly, this ma-

ture morphology was observed exclusively in neurons expressing NeuN alone at 28 dpi, when they have reached the inner and middle layers of the GCL and migration has already been completed.

Together, our observations that position, morphology, and markers show dramatic changes between 7 and 28 dpi, whereas the percentage of GFP$^+$ cells expressing neuronal markers does not increase (see Fig. 9*A–D*), indicate that the neuronal phenotype is determined by 7 dpi, but neuronal maturation occurs at a much slower pace, requiring several weeks.

The onset of glutamatergic connectivity: a late event in neuronal maturation

Glutamatergic PSCs were detected in GFP$^+$ neurons bearing GABAergic inputs from 18 dpi onwards (Fig. 6*A*). Notably, only 1 in 90 neurons studied showed glutamatergic but not GABAergic responses. Remarkably, neurons belonging to this functional group (GABA and glu) always displayed a mature excitability, because depolarizing current steps elicited repetitive spikes with large amplitude and high-frequency adaptation, a typical behavior of mature DGCs (Fig. 6*B*, Table 1). This developed excitability was also reflected in the large amplitudes of voltage-dependent inward Na^+ and outward K^+ currents (Fig. 6*C*). The AHP (AHP_{peak}, -5.8 ± 0.7; $n = 8$) was similar to that of neurons bearing only GABAergic afferents ($p > 0.05$) but smaller than in the GFP$^-$ controls (AHP_{peak}, -10.3 ± 0.9; $n = 8$; $p < 0.01$; Bonferroni's test), suggesting that other mechanisms are responsible for the onset of repetitive spiking.

Passive membrane properties in this group exhibited more mature characteristics, such as a significant increase in the membrane conductance normalized to C_m, indicating that the density of leak channels has increased compared with that of more immature neurons (Table 1). However, R_{input} and C_m were found to be different from those of unlabeled mature DGCs, because cells of different ages were pooled (Table 1). In fact, when neurons were grouped by age, these differences were reduced at 4 weeks and disappeared by 5 weeks (supplemental Fig. S1*A–C*, available at www.jneurosci.org as supplemental material).

Stimulation of the GCL induced complex PSCs that were partially blocked by BMI (blockade, $33.5 \pm 4.9\%$; $n = 8$) or kyn (blockade, $53.7 \pm 5.3\%$; $n = 15$) but fully abolished by the combination of BMI and kyn (blockade, $97.5 \pm 0.9\%$; $n = 4$). These results demonstrate the presence of both GABAergic and glutamatergic functional inputs (Fig. 6*D*). Furthermore, GABAergic spontaneous PSCs were observed in the presence of kyn and glutamatergic spontaneous PSCs in the presence of BMI (Fig. 6*E*,*F*), whereas no events were detected when both antagonists were applied together (data not shown). At this developmental stage, the frequency of GABA-mediated spontaneous PSCs (0.23 ± 0.06 Hz; $n = 7$) was significantly higher than that of neurons bearing GABAergic inputs only (0.05 ± 0.02 Hz; $n = 6$; $p < 0.03$).

Evoked glutamatergic PSCs were recorded in the presence of BMI and displayed rise and decay kinetics that are typical of fast glutamatergic transmission (Fig. 7*A*,*B*). Neurons displaying glutamatergic PSCs also possessed functional GABAergic inputs, consistent with the notion that GABAergic innervation precedes the onset of glutamatergic connectivity (see Fig. 9*E*). Interestingly, it was reported that early glutamatergic currents recorded from immature neurons of the adult DG were found to display a lower threshold for the induction of certain forms of glutamatergic long-term potentiation (Schmidt-Hieber et al., 2004), suggesting that they may be relevant to adult hippocampal function even before maturation has been fully completed.

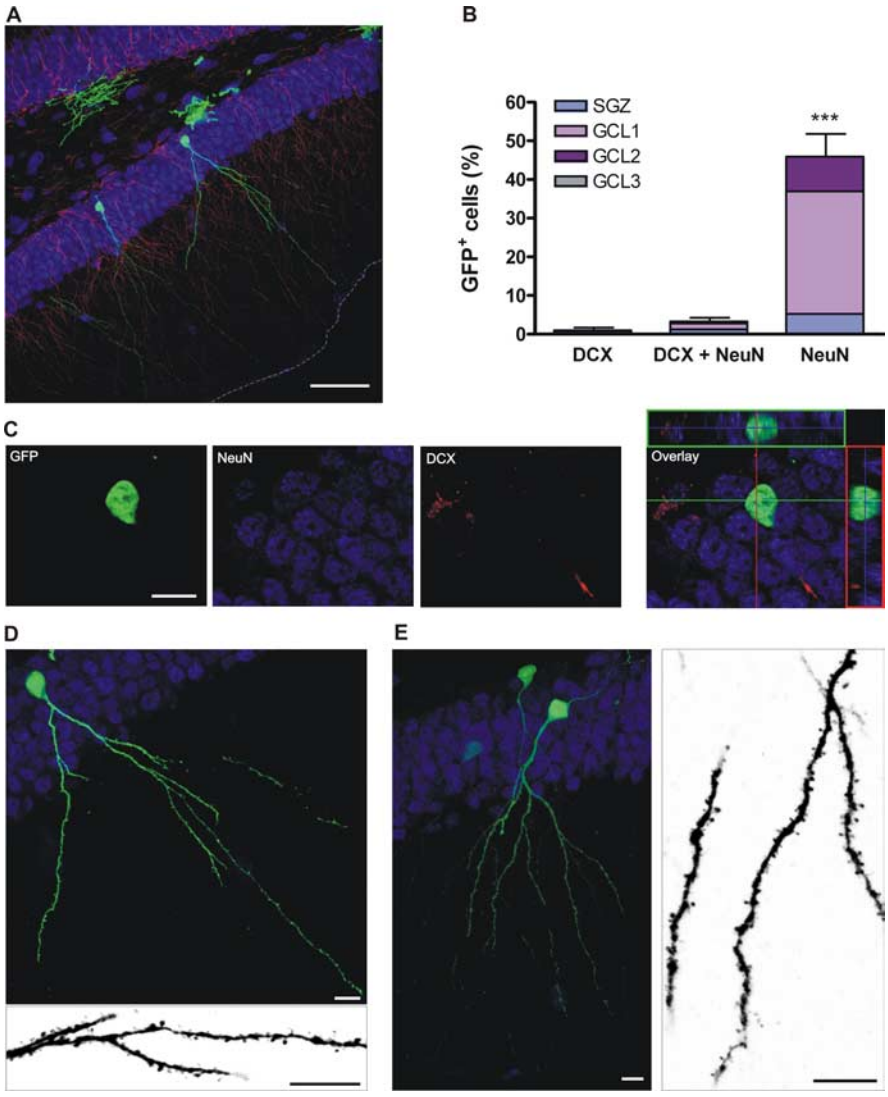

Figure 5. Morphological properties of class D neurons at 28 dpi. ***A***, Overview of the DG, merge of 34 optical sections. Scale bar, 50 μm. The border between the molecular layer and the ventricle is highlighted by a gray dashed line. ***B***, Distribution of GFP$^+$ cells expressing neuronal markers, normalized to the total number of GFP$^+$ cells. Bars show mean $\pm$ SEM percentage of cells expressing the corresponding marker ($n = 369$ GFP$^+$ cells from 6 mice). ***$p < 0.001$ by ANOVA with *post hoc* Bonferroni's test. ***C***, Single confocal plane of a neuron expressing NeuN, and the overlay with the orthogonal projections shown on the right. ***D***, Projection of 32 optical slices of a class D neuron. The image at the bottom is a merge of eight planes taken with a higher digital zoom displaying the details of dendritic spines. ***E***, Another example of class D neuron (merge of 28 confocal planes) and a magnified view extracted from a subset of nine planes shown on the right. Scale bars: ***C–E***, 10 μm.

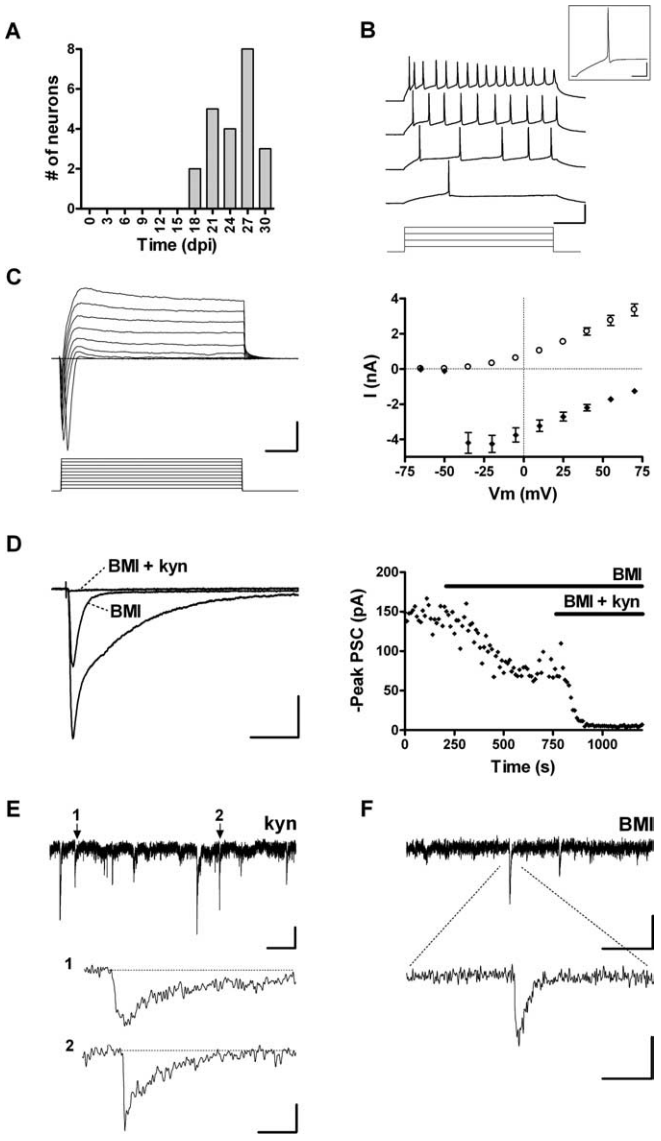

Figure 6. Functional properties of neurons with GABAergic and glutamatergic inputs. ***A***, Age of GFP$^+$ neurons with both GABAergic and glutamatergic afferents ($n = 24$). ***B***, Depolarizing current steps (20, 40, 50, and 100 pA) elicit repetitive spiking with frequency adaptation in an 18 dpi neuron. Calibration: 50 mV, 100 ms. A single spike from the second trace is shown in the inset. Calibration: 25 mV, 25 ms. ***C***, Left, Depolarizing voltage steps (15 mV) evoke fast inward and slow outward currents in an 18 dpi cell. Calibration: 2 nA, 5 ms. Right, *I–V* plot of peak inward Na^+ current (filled diamonds) and steady-state outward K^+ current (open circles). Data are mean ± SEM ($n = 23$). ***D***, Left, PSCs evoked in a 28 dpi neuron by GCL stimulation (20 V, 0.1 Hz) are fully blocked by BMI and kyn. Calibration: 40 pA, 50 ms. Right, Data from the neuron shown on the left displaying peak PSC amplitude before and during application of antagonists (depicted by the horizontal bars). ***E***, Spontaneous GABAergic PSCs with examples of events with slow (1) and fast (2) kinetics shown at a higher time resolution. Calibration: 5 pA, 2 s (top trace), 30 ms (traces 1 and 2). ***F***, Spontaneous glutamatergic PSCs. Calibration: 5 pA, 400 ms (top trace), 40 ms (bottom trace).

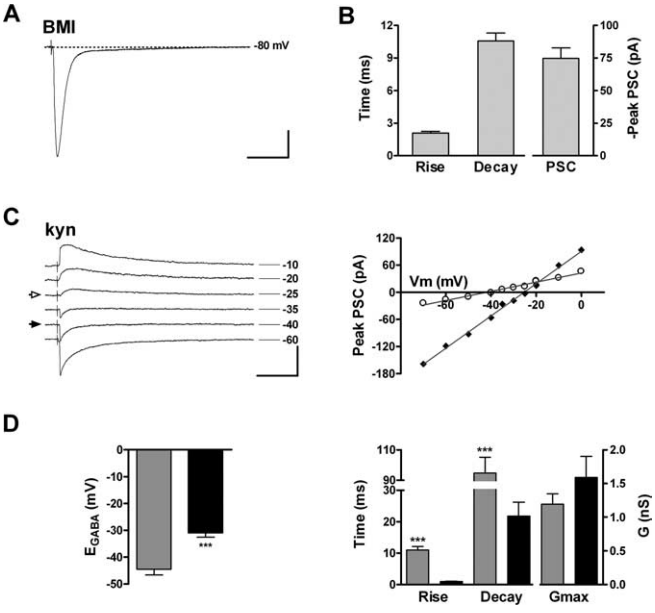

Figure 7. Properties of PSCs of GABA and glu neurons. ***A***, Glutamatergic PSC in an 18 dpi neuron evoked by stimulation of the GCL in the presence of BMI (20 μM). Calibration: 25 pA, 50 ms. ***B***, Kinetics and peak amplitude of glutamatergic PSCs ($n = 21$). ***C***, Left, GABAergic PSCs in a 27 dpi neuron evoked by stimulation of the GCL in the presence of kyn at V_{Hold} shown on the right. Pure fast/early and slow/late components are indicated with filled and open arrows. Calibration: 100 pA, 50 ms. Right, *I–V* curves of fast (filled diamonds) and slow (open circles) components of PSCs shown on the left, depicting distinct reversal potentials. ***D***, Left, Reversal potentials of fast (black) and slow (gray) currents recorded from 9 and 12 neurons, respectively. Right, Kinetics and maximal conductance of early and late components of GABAergic PSCs, measured at the reversal potential of the opposite component (see Materials and Methods). Data are mean ± SEM. ***$p < 0.0001$ (unpaired *t* test).

Maturation of GABAergic afferents in GABA and glu neurons

Evoked GABAergic PSCs were characterized in the presence of kyn. Current–voltage curves revealed two components with similar conductance (G_{max}): an early current with a depolarized E_{GABA} (−30.9 ± 1.6 mV; $n = 9$) and fast kinetics and a late current with a more hyperpolarized E_{GABA} and slow kinetics (−44.5 ± 2.1 mV; $n = 12$) (Fig. 7*C*,*D*). This difference in E_{GABA} for the fast and slow components is consistent with a gradient for the intracellular Cl^- concentration ($[Cl^-]$) between the somatic and dendritic compartments. In whole-cell recordings, ionic concentrations at the perisomatic cytoplasm are imposed by the patch pipette, whereas at more distal dendritic domains, Cl^- transporters are more effective at maintaining the intracellular $[Cl^-]$ at the physiological levels (Pearce, 1993; Jarolimek et al., 1999; Khirug et al., 2005). Therefore, our findings are in agreement with the fast perisomatic and slow dendritic responses observed in mature DGCs (Soltesz et al., 1995), in hippocampal pyramidal neurons (Pearce, 1993; Miles et al., 1996; Banks et al., 1998), and in cultured midbrain neurons (Jarolimek et al., 1999).

Perisomatic and dendritic GABAergic evoked PSCs could also be distinguished by focal application of BMI to restrict blockade of $GABA_A$ receptors to the soma of GFP$^+$ neurons (Fig. 8*A*) (Pearce, 1993; Banks et al., 1998). The fast component of evoked PSCs exhibited a striking and rapidly (<10 s) reversible blockade by focal somatic BMI treatment (Fig. 8*B*,*C*), whereas the remaining slow component was insensitive. Similar results were obtained in GFP$^-$ neurons (Fig. 8*C*). The slow component of evoked PSCs in GFP$^+$ neurons was fully blocked by bath-applied BMI, confirming that this component is also mediated by $GABA_A$ receptors (Fig. 8*D*). These observations strengthen our conclusion that fast GABAergic currents arise from perisomatic synapses, whereas slow events are of dendritic origin. The kinetic differences between slow dendritic and fast perisomatic PSCs might be attributable to the composition of postsynaptic receptor subunits (Pearce, 1993; Banks et al., 1998) and/or to dendritic filtering (Soltesz et al., 1995). It is also important to note that dendritic and somatic inhibition is exerted by distinct types of GABAergic interneurons, which seem to control different func-

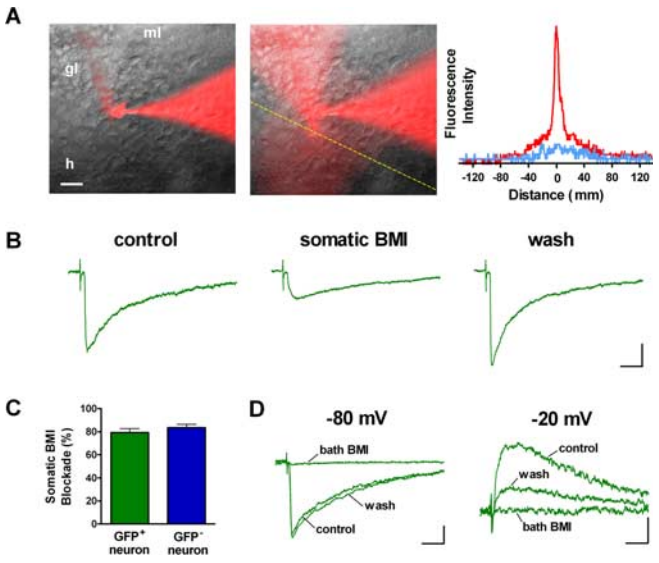

Figure 8. Somatic blockade of fast GABAergic evoked PSCs. ***A***, Merged fluorescent and bright-field images before (left) and during (middle) focal application of BMI in a whole-cell recording, with Alexa Fluor 594 included in the recording and puffing pipettes. ml, Molecular layer; gl, granule layer; h, hilus. Fluorescence intensity (arbitrary units) measured at the yellow dashed line before (blue) and during (red) BMI perfusion is shown to the right. ***B***, GABAergic-evoked PSCs recorded before (control), during (somatic BMI), and after (wash) somatic application of BMI onto a GFP$^+$ neuron with both GABA and glutamate inputs recorded at $V_{hold} = -80$ mV. Calibration: 10 pA, 20 ms. ***C***, Somatic blockade of evoked PSCs was significant for GFP$^+$ ($p < 0.002$; $n = 3$; single-sample *t* test) and GFP$^-$ DGCs ($p < 0.002$; $n = 3$). Bars represent mean ± SEM. ***D***, Bath application of BMI blocks the slow component of GABAergic PSCs that predominates at $V_{hold} = -20$ mV and the mixed fast/slow responses recorded at $V_{hold} = -80$ mV in the same GFP$^+$ neuron (percentage blockade at −80 mV, 97.7 ± 0.8%; $n = 4$; $p < 0.0001$; single-sample *t* test). Calibration: 25 pA, 20 ms. All recordings shown in this figure were performed in the presence of kyn (4 mM).

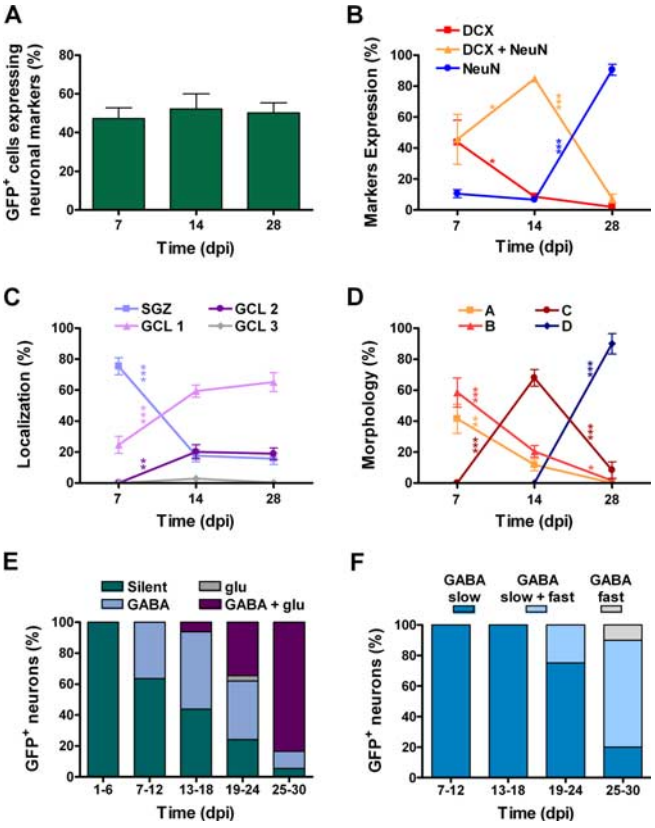

Figure 9. Time course of neurogenesis, morphology, migration, and synaptogenesis. ***A***, Neurogenesis quantified as the percentage of GFP$^+$ cells that express any combination of neuronal markers. No significant differences were observed ($p = 0.86$; ANOVA). Bars represent mean ± SEM. ***B***, ***C***, ***D***, Time courses of the expression of neuronal markers, distribution, and morphology normalized to the total number of GFP$^+$ neurons. Data are mean ± SEM, calculated as the percentage for each mouse averaged at each time point. ***B–D***, Sample size: 154, 208, and 192 neurons (***B***, ***C***) and 64, 88, and 39 (***D***) for 7, 14, and 28 dpi, respectively. Changes were analyzed for each variable using one-way ANOVA followed by a Bonferroni's *post hoc* test for adjacent intervals. *$p < 0.05$; **$p < 0.01$; ***$p < 0.001$. ***E***, Incidence of GABAergic and glutamatergic inputs normalized to the total number of GFP$^+$ neurons for each time bin ($n = 84$). ***F***, Percentage of GFP$^+$ neurons bearing slow and/or fast GABAergic inputs, normalized to the number of GFP$^+$ neurons with GABAergic inputs for each bin ($n = 62$).

tional aspects of principal neurons (Freund and Buzsaki, 1996; Miles et al., 1996).

The study of spontaneous synaptic responses also evidenced two populations of GABAergic spontaneous PSCs with fast and slow kinetics in GFP$^+$ neurons and also in GFP$^-$ controls at $V_{hold} = -80$ mV, similar to mature hippocampal neurons (Soltesz et al., 1995; Banks et al., 1998). Interestingly, fast spontaneous PSCs that were literally absent in immature neurons lacking glutamatergic inputs became dominant in neurons bearing both GABA and glu afferents (supplemental Fig. S2*A*,*B*, available at www.jneurosci.org as supplemental material). To determine whether fast and slow GABAergic spontaneous PSCs arise from different cellular compartments, recordings were performed in symmetric Cl^-, a condition that imposes an E_{GABA} of 0 mV for perisomatic synaptic responses (Pearce, 1993). Accordingly, only slow spontaneous PSCs could be detected at $V_{hold} = 0$ mV, further supporting the perisomatic nature of fast synaptic events and the more distant (dendritic) localization of slow responses (supplemental Fig. S2*C*,*D*, available at www.jneurosci.org as supplemental material).

It is important to note that glutamatergic afferents were detected in neurons with mature excitability and morphology that also possessed GABAergic inputs (Fig. 9*E*). In addition, fast GABAergic PSCs were only found in neurons bearing functional glutamatergic inputs (Fig. 9*F*). However, 4 of 13 neurons with glutamatergic afferents failed to exhibit fast GABAergic currents, strongly suggesting a later arrival of GABAergic perisomatic contacts. Together, our findings support the notion that the development of afferent synaptic connections takes ~4 weeks and follows the sequence: silent → slow GABA → glu → fast GABA.

Discussion

The question of how neurons develop in the adult DG was examined using a retrovirus that expresses GFP in the progeny of dividing progenitor cells and monitoring changes in morphology, localization, expression of neuronal markers, and electrophysiological properties of individual neurons of a known maximal age. In this way, we identified discrete stages in the maturation of adult-born DGCs (Fig. 10). During the first week, neurons located in the SGZ show processes parallel to the GCL and display small spikes but lack synaptic afferents. One week later, neurons exhibit spineless dendrites that reach the inner molecular layer and receive functional GABAergic contacts. By the fourth week, neurons are established in their final position and have developed spiny dendrites reaching the outer molecular layer. At this stage, functional glutamatergic afferents become abundant and action potentials exhibit high frequency adaptation. Maturation is finally completed with the onset of perisomatic GABAergic contacts. This sequence for the establishment of afferent connectivity closely resembles that of hippocampal development.

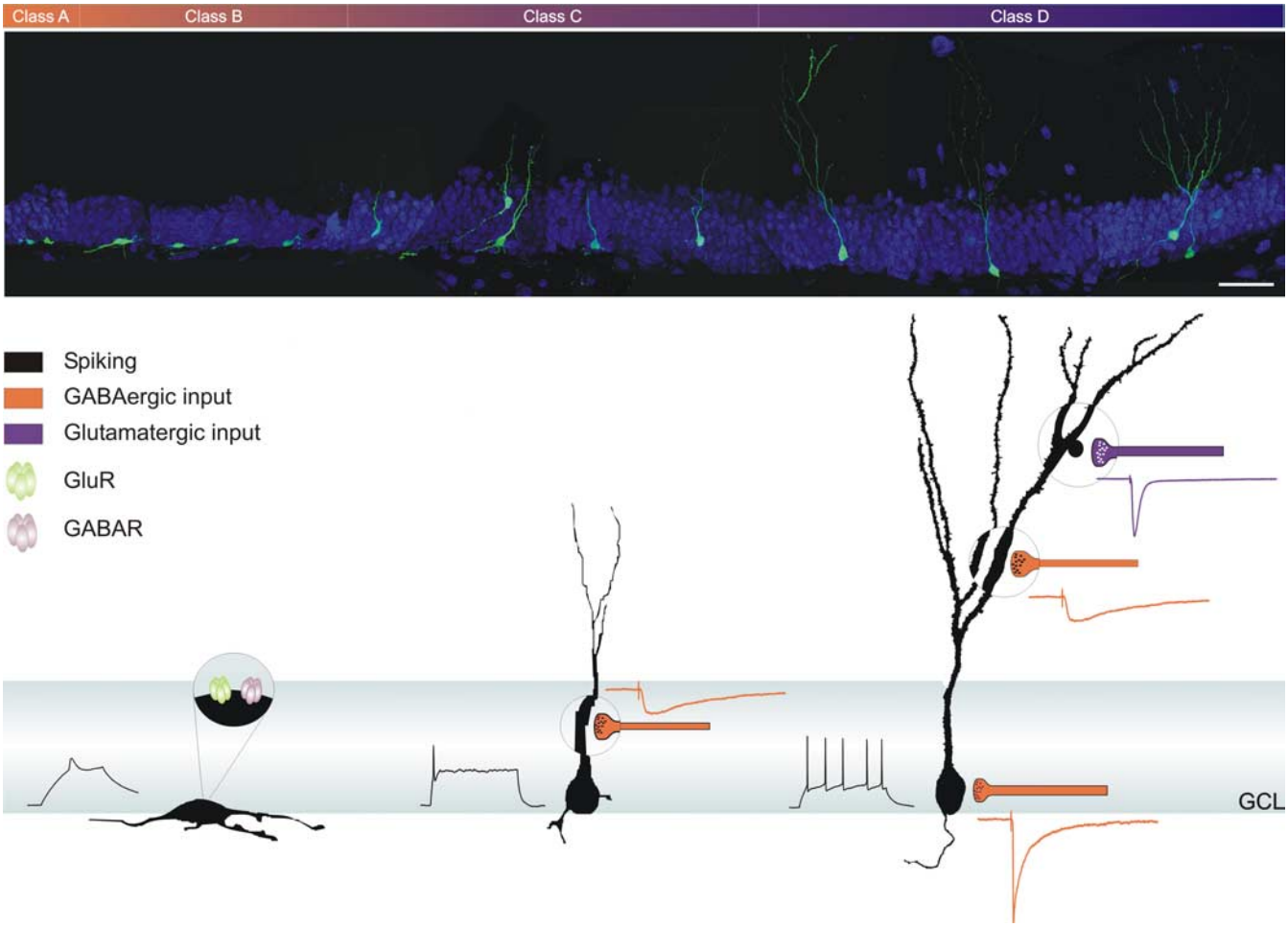

Figure 10. Overview of the development of a new DGC in the adult hippocampus. Top, Montage of 11 confocal images, each taken from projections of 16–30 optical slices. Scale bar, 50 μm. Bottom, Schematic representation of developmental hallmarks of morphology, excitability, and afferent synaptic connectivity with their corresponding postsynaptic currents.

Neuronal migration and maturation in the GCL

The fraction of GFP$^+$ cells expressing neuronal markers showed almost no variation between 7 and 28 dpi (Fig. 9*A*), consistent with an early determination of the neuronal phenotype (Kempermann et al., 2003). Accordingly, electrophysiological recordings revealed immature action potentials as early as 1 dpi (Fig. 2*A*). In contrast, a delayed maturation was observed in few neurons (<10%) that still expressed DCX and showed immature morphology at 28 dpi and in silent neurons recorded at ~20 dpi (Fig. 9*B*,*D*,*E*). This late maturation might reflect neurons that develop at a slower pace or, alternatively, neurons that derive from NPCs that divided a few more times or remained quiescent before acquiring a neuronal fate.

The overlapping expression of DCX and NeuN between 7 and 14 dpi together with the conspicuous morphological maturation found during this interval indicates that each individual marker provides little information about the degree of maturation (Fig. 9*B*). For instance, neurons expressing DCX and NeuN showed a class A or B morphology at 7 dpi but a class C phenotype at 14 dpi. Likewise, neurons expressing NeuN exhibited a class D morphology at 28 dpi but not at earlier stages. Therefore, neuronal markers and morphology are both required to discriminate distinct stages of neuronal maturity.

Adult-born neurons showed remarkable migration from the SGZ toward GCL 1/2 between 7 and 14 dpi, when DCX expression was highest (Fig. 9*B*,*C*) (Brown et al., 2003). Interestingly, little migration occurred from 14 to 28 dpi, and almost no neurons reached GCL 3. Although migration to the deeper layers may exceed the interval studied here, the lack of DCX expression at 28 dpi strongly suggests that migration has ended at that point. Accordingly, it has been shown that the proportions of BrdU-labeled cells found throughout the different layers of the DG do not change significantly between 1 and 11 months (Kempermann et al., 2003). Together, these results suggest that adult neurogenesis might contribute preferentially to the inner and middle layers of the GCL.

GABAergic afferents and neuronal maturation

GABAergic inputs show an early onset and undergo dramatic changes during neuronal maturation (Figs. 4, 7, 9*E*,*F*) (supplemental Fig. S2, available at www.jneurosci.org as supplemental material). In immature neurons, E_{GABA} was found to be close to the depolarized E_{Cl^-} imposed by the patch pipette (Fig. 4*E*), which suggests two possible scenarios: (1) early GABAergic connections are formed at or near the soma; and 2) these afferents are dendritic, and either the dendritic [Cl^-] of compact immature neurons is effectively imposed by the patch electrode or intracellular [Cl^-] is physiologically high, which is typical for developing neurons in which E_{GABA} is known to be depolarizing (Rivera et al., 1999). A dendritic origin seems more plausible, because the rise time of evoked PSCs recorded from immature neurons (10.1 ± 0.8 ms; $n = 24$) (Fig. 4*F*) was remarkably similar to that

of dendritic responses recorded in neurons bearing fast perisomatic and slow dendritic inputs (11.0 ± 1.1 ms; $n = 12$; $p = 0.5$) (Fig. 7*D*). In addition, there is no reported evidence of perisomatic events with such a slow time course.

We observed two discrete stages in the development of GABAergic neurotransmission. Slow responses (most likely of dendritic origin) appear in early immature neurons, whereas fast perisomatic inputs are only detected at a much later developmental stage, once glutamatergic terminals are impinging onto dendritic spines. The separate onsets of slow and fast GABAergic inputs may underscore a difference in their putative roles on neuronal maturation. For instance, GABAergic transmission is known to play a trophic role during embryonic and early postnatal development (LoTurco et al., 1995; Marty et al., 1996; Ganguly et al., 2001; Ben Ari, 2002). However, the mechanisms underlying neuronal maturation in the adult DG remain unknown, and it seems crucial to understand whether early GABA is required in this process. In contrast, the late onset of perisomatic GABA makes it an unlikely modulator for neuronal maturation. Rather, it is tempting to speculate that perisomatic GABAergic inputs, which are known to influence neuronal output (Freund, 2003), might become critical as an inhibitory control only after excitation becomes physiologically relevant.

Similarities between the developing and adult hippocampus

The developmental timing observed here is in agreement with a recent report in which ~2-week-old neurons of the adult DG, labeled using enhanced GFP under control of the proopiomelanocortin promoter, showed immature spikes and morphology and receive GABAergic but not glutamatergic inputs (Overstreet Wadiche et al., 2005). In addition, the mature DGC morphology found at 28 dpi is consistent with previous findings obtained with a different methodology (Seri et al., 2001). Our results also present conclusive evidence supporting the recent observations that adult DGCs with high R_{input} display only GABA-mediated afferents (Ambrogini et al., 2004), and that adult hippocampal NPCs expressing GFP under the nestin promoter exhibit GABAergic currents (Wang et al., 2005).

It is striking that the sequence of events observed in the adult DG is also followed during hippocampal development. Tyzio et al. (1999) showed that spiking CA1 pyramidal neurons in the neonatal hippocampus can be either silent, show GABAergic PSCs, or show both GABA and glu inputs, strongly suggesting the silent neuron → GABA → glu sequence of excitability and afferent connectivity. The same sequence was observed in CA1 pyramidal neurons of the embryonic macaque (Khazipov et al., 2001) and in CA1 GABAergic interneurons of embryonic rats (Hennou et al., 2002). In contrast, the order of appearance of fast and slow GABAergic afferents in the developing hippocampus has not been clearly established. Although the existence of principal neurons displaying exclusively slow GABAergic PSCs has not yet been confirmed by electrophysiological recordings in the developing hippocampus (Hollrigel and Soltesz, 1997; Banks et al., 2002), anatomical studies indicate that dendritic GABAergic synapses are formed before somatic ones. In a previous study, Lübbers and Frotscher (1988) showed that immature DGCs in P5 rats received mostly GABAergic afferents impinging onto dendritic shafts. Similar findings were reported for CA1 pyramidal neurons (Dupuy and Houser, 1996; Tyzio et al., 1999; Hennou et al., 2002; Gozlan and Ben Ari, 2003). In addition, perisomatic GABAergic synapses seem to be the latest to be assembled in the developing hippocampus, given that interneurons responsible for perisomatic inhibition are not yet functional at birth in the CA1 area (Gozlan and Ben Ari, 2003). Perisomatic inhibitory interneurons of the DG exhibit active migration and only reach their final destination in the GCL by P30, evidencing dynamic rearrangements in the GABAergic circuitry during postnatal development (Dupuy-Davies and Houser, 1999; Morozov and Freund, 2003). Our data demonstrate that perisomatic inhibition is the latest to appear in the adult DG (Fig. 9*F*) despite the fact that interneurons responsible for perisomatic innervation are fully functional at this stage. The finding that the developmental sequence for neuronal maturation in the developing and adult brain is preserved in environments that are so distinct suggests that such sequence is primarily determined by a cell-autonomous program rather than by environmental cues.

The similarities between developmental and adult neurogenesis do not occur in the OB. During development, neurons can spike well before the onset of synaptogenesis. During adulthood, however, synaptogenesis precedes the onset of excitability, and both processes occur once migration to the OB has ended (Belluzzi et al., 2003; Carleton et al., 2003). Therefore, not only is the maturation of neuronal function in the adult OB different from what occurs during development, but it is also distinct from the process observed in the adult DG. It remains to be elucidated whether these differences respond to intrinsic properties of NPCs or to environmental cues of the OB versus DG.

Great efforts are currently being devoted to study the influence of behavior on the rate of adult neurogenesis and the physiological relevance of adult neurogenesis in hippocampal function (van Praag et al., 2000; Shors et al., 2001; Madsen et al., 2003; Santarelli et al., 2003; Schinder and Gage, 2004). In this context, the time course described here for the neuronal maturation (~3–4 weeks) seems extremely slow as a mechanism for plasticity, because it can only modify hippocampal circuits several weeks after neuronal differentiation was initiated. Hence, regulation of neurogenesis by a learning task would not alter the performance of the animal during that particular event, but it might be crucial for maintaining a level of hippocampal plasticity that is required for future tasks. Consequently, additional checkpoints for the control of neuronal connectivity might provide faster mechanisms of plasticity that would only require hours or days, such as integrating a "readily connectable neuron" into a circuit that is avid of new functional units.

References

Altman J, Bayer SA (1990) Migration and distribution of two populations of hippocampal granule cell precursors during the perinatal and postnatal periods. J Comp Neurol 301:365–381.

Alvarez-Buylla A, Seri B, Doetsch F (2002) Identification of neural stem cells in the adult vertebrate brain. Brain Res Bull 57:751–758.

Ambrogini P, Lattanzi D, Ciuffoli S, Agostini D, Bertini L, Stocchi V, Santi S, Cuppini R (2004) Morpho-functional characterization of neuronal cells at different stages of maturation in granule cell layer of adult rat dentate gyrus. Brain Res 1017:21–31.

Angevine Jr JB (1965) Time of neuron origin in the hippocampal region. An autoradiographic study in the mouse. Exp Neurol Suppl 2:1–70.

Banks MI, Li TB, Pearce RA (1998) The synaptic basis of $GABA_A$, slow. J Neurosci 18:1305–1317.

Banks MI, Hardie JB, Pearce RA (2002) Development of $GABA_A$ receptor-mediated inhibitory postsynaptic currents in hippocampus. J Neurophysiol 88:3097–3107.

Barry PH, Lynch JW (1991) Liquid junction potentials and small cell effects in patch-clamp analysis. J Membr Biol 121:101–117.

Bayer SA, Yackel JW, Puri PS (1982) Neurons in the rat dentate gyrus granular layer substantially increase during juvenile and adult life. Science 216:890–892.

Belluzzi O, Benedusi M, Ackman J, LoTurco JJ (2003) Electrophysiological

differentiation of new neurons in the olfactory bulb. J Neurosci 23:10411–10418.
Ben Ari Y (2002) Excitatory actions of GABA during development: the nature of the nurture. Nat Rev Neurosci 3:728–739.
Brown JP, Couillard-Despres S, Cooper-Kuhn CM, Winkler J, Aigner L, Kuhn HG (2003) Transient expression of doublecortin during adult neurogenesis. J Comp Neurol 467:1–10.
Cameron HA, McKay RD (2001) Adult neurogenesis produces a large pool of new granule cells in the dentate gyrus. J Comp Neurol 435:406–417.
Carleton A, Petreanu LT, Lansford R, Alvarez-Buylla A, Lledo PM (2003) Becoming a new neuron in the adult olfactory bulb. Nat Neurosci 6:507–518.
Duman RS (2004) Depression: a case of neuronal life and death? Biol Psychiatry 56:140–145.
Dupuy ST, Houser CR (1996) Prominent expression of two forms of glutamate decarboxylase in the embryonic and early postnatal rat hippocampal formation. J Neurosci 16:6919–6932.
Dupuy-Davies S, Houser CR (1999) Evidence for changing positions of GABA neurons in the developing rat dentate gyrus. Hippocampus 9:186–199.
Freund TF (2003) Interneuron diversity series: rhythm and mood in perisomatic inhibition. Trends Neurosci 26:489–495.
Freund TF, Buzsaki G (1996) Interneurons of the hippocampus. Hippocampus 6:347–470.
Gage FH (2000) Mammalian neural stem cells. Science 287:1433–1438.
Ganguly K, Schinder AF, Wong ST, Poo M (2001) GABA itself promotes the developmental switch of neuronal GABAergic responses from excitation to inhibition. Cell 105:521–532.
Garcia AD, Doan NB, Imura T, Bush TG, Sofroniew MV (2004) GFAP-expressing progenitors are the principal source of constitutive neurogenesis in adult mouse forebrain. Nat Neurosci 7:1233–1241.
Gleeson JG, Lin PT, Flanagan LA, Walsh CA (1999) Doublecortin is a microtubule-associated protein and is expressed widely by migrating neurons. Neuron 23:257–271.
Gozlan H, Ben Ari Y (2003) Interneurons are the source and the targets of the first synapses formed in the rat developing hippocampal circuit. Cereb Cortex 13:684–692.
Hennou S, Khalilov I, Diabira D, Ben Ari Y, Gozlan H (2002) Early sequential formation of functional $GABA_A$ and glutamatergic synapses on CA1 interneurons of the rat fetal hippocampus. Eur J Neurosci 16:197–208.
Hollrigel GS, Soltesz I (1997) Slow kinetics of miniature IPSCs during early postnatal development in granule cells of the dentate gyrus. J Neurosci 17:5119–5128.
Jarolimek W, Lewen A, Misgeld U (1999) A furosemide-sensitive K^+-Cl^- cotransporter counteracts intracellular Cl^- accumulation and depletion in cultured rat midbrain neurons. J Neurosci 19:4695–4704.
Jones SP, Rahimi O, O'Boyle MP, Diaz DL, Claiborne BJ (2003) Maturation of granule cell dendrites after mossy fiber arrival in hippocampal field CA3. Hippocampus 13:413–427.
Kaila K (1994) Ionic basis of $GABA_A$ receptor channel function in the nervous system. Prog Neurobiol 42:489–537.
Kempermann G, Gast D, Kronenberg G, Yamaguchi M, Gage FH (2003) Early determination and long-term persistence of adult-generated new neurons in the hippocampus of mice. Development 130:391–399.
Khazipov R, Esclapez M, Caillard O, Bernard C, Khalilov I, Tyzio R, Hirsch J, Dzhala V, Berger B, Ben Ari Y (2001) Early development of neuronal activity in the primate hippocampus *in utero*. J Neurosci 21:9770–9781.
Khirug S, Huttu K, Ludwig A, Smirnov S, Voipio J, Rivera C, Kaila K, Khiroug L (2005) Distinct properties of functional KCC2 expression in immature mouse hippocampal neurons in culture and in acute slices. Eur J Neurosci 21:899–904.
Kokaia Z, Lindvall O (2003) Neurogenesis after ischaemic brain insults. Curr Opin Neurobiol 13:127–132.
Laurie DJ, Wisden W, Seeburg PH (1992) The distribution of thirteen $GABA_A$ receptor subunit mRNAs in the rat brain. III. Embryonic and postnatal development. J Neurosci 12:4151–4172.
Liu S, Wang J, Zhu D, Fu Y, Lukowiak K, Lu YM (2003) Generation of functional inhibitory neurons in the adult rat hippocampus. J Neurosci 23:732–736.
Lois C, Alvarez-Buylla A (1994) Long-distance neuronal migration in the adult mammalian brain. Science 264:1145–1148.
LoTurco JJ, Owens DF, Heath MJ, Davis MB, Kriegstein AR (1995) GABA and glutamate depolarize cortical progenitor cells and inhibit DNA synthesis. Neuron 15:1287–1298.
Lübbers K, Frotscher M (1988) Differentiation of granule cells in relation to GABAergic neurons in the rat fascia dentata. Combined Golgi/EM and immunocytochemical studies. Anat Embryol (Berl) 178:119–127.
Madsen TM, Kristjansen PE, Bolwig TG, Wortwein G (2003) Arrested neuronal proliferation and impaired hippocampal function following fractionated brain irradiation in the adult rat. Neuroscience 119:635–642.
Marty S, Berninger B, Carroll P, Thoenen H (1996) GABAergic stimulation regulates the phenotype of hippocampal interneurons through the regulation of brain-derived neurotrophic factor. Neuron 16:565–570.
McCabe BK, Silveira DC, Cilio MR, Cha BH, Liu X, Sogawa Y, Holmes GL (2001) Reduced neurogenesis after neonatal seizures. J Neurosci 21:2094–2103.
Miles R, Toth K, Gulyas AI, Hajos N, Freund TF (1996) Differences between somatic and dendritic inhibition in the hippocampus. Neuron 16:815–823.
Morozov YM, Freund TF (2003) Postnatal development and migration of cholecystokinin-immunoreactive interneurons in rat hippocampus. Neuroscience 120:923–939.
Mullen RJ, Buck CR, Smith AM (1992) NeuN, a neuronal specific nuclear protein in vertebrates. Development 116:201–211.
Nottebohm F (2002) Neuronal replacement in adult brain. Brain Res Bull 57:737–749.
Overstreet Wadiche LS, Bromberg DA, Bensen AL, Westbrook GL (2005) GABAergic signaling to newborn neurons in dentate gyrus. J Neurophysiol, in press.
Owens DF, Boyce LH, Davis MB, Kriegstein AR (1996) Excitatory GABA responses in embryonic and neonatal cortical slices demonstrated by gramicidin perforated-patch recordings and calcium imaging. J Neurosci 16:6414–6423.
Parent JM, Lowenstein DH (2002) Seizure-induced neurogenesis: are more new neurons good for an adult brain? Prog Brain Res 135:121–131.
Parent JM, Yu TW, Leibowitz RT, Geschwind DH, Sloviter RS, Lowenstein DH (1997) Dentate granule cell neurogenesis is increased by seizures and contributes to aberrant network reorganization in the adult rat hippocampus. J Neurosci 17:3727–3738.
Pearce RA (1993) Physiological evidence for two distinct $GABA_A$ responses in rat hippocampus. Neuron 10:189–200.
Rivera C, Voipio J, Payne JA, Ruusuvuori E, Lahtinen H, Lamsa K, Pirvola U, Saarma M, Kaila K (1999) The K^+/Cl^- co-transporter KCC2 renders GABA hyperpolarizing during neuronal maturation. Nature 397:251–255.
Santarelli L, Saxe M, Gross C, Surget A, Battaglia F, Dulawa S, Weisstaub N, Lee J, Duman R, Arancio O, Belzung C, Hen R (2003) Requirement of hippocampal neurogenesis for the behavioral effects of antidepressants. Science 301:805–809.
Schinder AF, Gage FH (2004) A hypothesis about the role of adult neurogenesis in hippocampal function. Physiology (Bethesda) 19:253–261.
Schmidt-Hieber C, Jonas P, Bischofberger J (2004) Enhanced synaptic plasticity in newly generated granule cells of the adult hippocampus. Nature 429:184–187.
Seri B, Garcia-Verdugo JM, McEwen BS, Alvarez-Buylla A (2001) Astrocytes give rise to new neurons in the adult mammalian hippocampus. J Neurosci 21:7153–7160.
Shors TJ, Miesegaes G, Beylin A, Zhao M, Rydel T, Gould E (2001) Neurogenesis in the adult is involved in the formation of trace memories. Nature 410:372–376.
Soltesz I, Smetters DK, Mody I (1995) Tonic inhibition originates from synapses close to the soma. Neuron 14:1273–1283.
Song HJ, Stevens CF, Gage FH (2002) Neural stem cells from adult hippocampus develop essential properties of functional CNS neurons. Nat Neurosci 5:438–445.
Super H, Soriano E (1994) The organization of the embryonic and early postnatal murine hippocampus. II. Development of entorhinal, commissural, and septal connections studied with the lipophilic tracer DiI. J Comp Neurol 344:101–120.
Tanaka T, Serneo FF, Tseng HC, Kulkarni AB, Tsai LH, Gleeson JG (2004) Cdk5 phosphorylation of doublecortin ser297 regulates its effect on neuronal migration. Neuron 41:215–227.
Toda H, Takahashi J, Mizoguchi A, Koyano K, Hashimoto N (2000) Neurons generated from adult rat hippocampal stem cells form func-

tional glutamatergic and GABAergic synapses in vitro. Exp Neurol 165:66–76.

Tyzio R, Represa A, Jorquera I, Ben Ari Y, Gozlan H, Aniksztejn L (1999) The establishment of GABAergic and glutamatergic synapses on CA1 pyramidal neurons is sequential and correlates with the development of the apical dendrite. J Neurosci 19:10372–10382.

Tyzio R, Ivanov A, Bernard C, Holmes GL, Ben Ari Y, Khazipov R (2003) Membrane potential of CA3 hippocampal pyramidal cells during postnatal development. J Neurophysiol 90:2964–2972.

van Praag H, Kempermann G, Gage FH (1999) Running increases cell proliferation and neurogenesis in the adult mouse dentate gyrus. Nat Neurosci 2:266–270.

van Praag H, Kempermann G, Gage FH (2000) Neural consequences of environmental enrichment. Nat Rev Neurosci 1:191–198.

van Praag H, Schinder AF, Christie BR, Toni N, Palmer TD, Gage FH (2002) Functional neurogenesis in the adult hippocampus. Nature 415:1030–1034.

Wang LP, Kempermann G, Kettenmann H (2005) A subpopulation of precursor cells in the mouse dentate gyrus receives synaptic GABAergic input. Mol Cell Neurosci 29:181–189.

Xu L, Yee JK, Wolff JA, Friedmann T (1989) Factors affecting long-term stability of Moloney murine leukemia virus-based vectors. Virology 171:331–341.

Ye GL, Yi S, Gamkrelidze G, Pasternak JF, Trommer BL (2005) AMPA and NMDA receptor-mediated currents in developing dentate gyrus granule cells. Brain Res Dev Brain Res 155:26–32.

Zhang ZW (2004) Maturation of layer V pyramidal neurons in the rat prefrontal cortex: intrinsic properties and synaptic function. J Neurophysiol 91:1171–1182.